Feasibility region analysis of active systems: investigating the lateral performance envelope of sports cars

Taylor & Francis
Taylor & Francis Group

Vehicle System Dynamics
International Journal of Vehicle Mechanics and Mobility

ISSN: 0042-3114 (Print) 1744-5159 (Online) Journal homepage: www.tandfonline.com/journals/nvsd20

Feasibility region analysis of active systems: investigating the lateral performance envelope of sports cars

Roberto Aratri, Giuseppe Guastadisegni, Stefano De Pinto, Arnau Doria-Cerezo, Aldo Sorniotti, Francesco Bottiglione & Giacomo Mantriota

To cite this article: Roberto Aratri, Giuseppe Guastadisegni, Stefano De Pinto, Arnau Doria-Cerezo, Aldo Sorniotti, Francesco Bottiglione & Giacomo Mantriota (2025) Feasibility region analysis of active systems: investigating the lateral performance envelope of sports cars, Vehicle System Dynamics, 63:9, 1676-1697, DOI: 10.1080/00423114.2024.2379546

To link to this article: https://doi.org/10.1080/00423114.2024.2379546

Published online: 23 Jul 2024.

VEHICLE SYSTEM DYNAMICS
2025, VOL. 63, NO. 9, 1676–1697
https://doi.org/10.1080/00423114.2024.2379546

Feasibility region analysis of active systems: investigating the lateral performance envelope of sports cars

Roberto Aratri[a], Giuseppe Guastadisegni[b,c], Stefano De Pinto[c], Arnau Doria-Cerezo[d], Aldo Sorniotti[e], Francesco Bottiglione[a] and Giacomo Mantriota[a]

[a]Dipartimento di Meccanica Matematica Management, Politecnico di Bari, Bari, Italy; [b]Department of Mechanical Engineering Sciences, University of Surrey, Guildford, UK; [c]McLaren Automotive Europe, Polígono Industrial L'Albornar, Santa Oliva, Spain; [d]Institut d'Organització i Control de Sistemes Industrials, Universitat Politecnica de Catalunya, Barcelona, Spain; [e]Department of Mechanical and Aerospace Engineering, Polytechnic University of Turin, Turin, Italy

ABSTRACT

Active systems are gaining significant importance because of their ability of enhancing handling performance, stability, and driver engagement, especially in sports cars. The upfront study of the achievable handling characteristics with a specific actuator set is crucial, given the involved development costs and time. In this context, although several recent studies have compared the cornering response associated with different chassis actuations, none of them has analysed in detail the resulting performance envelope, i.e. the feasibility region, based on the operating limit of the available hardware. This study targets the identified gap and presents a methodology for obtaining the feasibility region of chassis actuation systems, defined as the locus of the achievable understeer characteristics. The analysis considers front and rear active camber (FAC and RAC), rear-wheel-steering (RWS) and variable roll moment distribution (RMD). Simplified vehicle models with reduced number of degrees of freedom (DoFs) and other features to accurately obtain the feasibility region and the relevant dynamic response indicators in the early design stages of the vehicle are compared with a high-fidelity model based on VI-CarRealTime. The results highlight the favourable trade-off between complexity and accuracy of a 3-DoF nonlinear model accounting for suspension kinematics and compliances.

ARTICLE HISTORY
Received 23 November 2023
Revised 18 May 2024
Accepted 6 July 2024

KEYWORDS
Active vehicle system development; chassis control system performance; cornering response; handling performance envelope; feasibility region analysis; key performance indicators

1. Introduction

Passenger cars tend to be equipped with a growing array of chassis actuators, such as electro-hydraulic or electro-mechanical friction brakes, active and semi-active suspensions with variable roll moment distribution (RMD) capability, and rear-wheel-steering (RWS). These actuators vary the lateral, longitudinal, and/or vertical tyre forces, and thus enhance vehicle dynamics and active safety [1]. In particular, active camber (AC) and RWS modify the lateral forces [2–4]. In specific vehicle architectures, the powertrain works as a chassis actuator by enabling controllable distribution of the wheel torque and thus the longitudinal

CONTACT Giuseppe Guastadisegni giuseppe.guastadisegni@surrey.ac.uk

tyre force, commonly referred to as torque vectoring [4–7]. Controllable RMD varies the vertical load transfer distribution between the axles [8], which has an indirect impact over the lateral forces and slip angles. For example, Ricco et al. [8] present a front-to-rear RMD controller, which increases the maximum lateral acceleration without altering the linear region of the understeer characteristic. Especially in high-performance vehicles, there is also the possibility, often referred to as active wheel alignment [9,10], of controlling the entire wheel corner kinematics, by concurrently modifying the wheel camber and steering angles.

The current trend is to equip production sports cars with multiple actuators to simultaneously enhance cornering performance and safety, e.g. see the Ferrari SF90 and Purosangue, McLaren Artura and Lamborghini Revuelto, and the multitude of studies on chassis control integration [11–20]. Porsche Engineering [12,13] integrates RWS with torque vectoring through approaches that reduce the intervention of the feedback control contributions and promote feedforward model-based control. This avoids a 'synthetic feeling' that could negatively impact the driving experience. A similar approach is proposed by Chien et al. [14], where a fuzzy logic algorithm performs a smooth blending between a feedforward handling-oriented contribution, and a feedback strategy targeting stabilisation and safety. In parallel, it is becoming increasingly important to improve energy efficiency. For example, in electric and hybrid vehicles, integrated systems can maximise energy recovery during braking through active aerodynamics, friction brakes and electric motor torque distribution [20]. In [21], the vehicle understeer characteristics and wheel torque distribution are designed to minimise the relevant power losses, and, consequently, achieve energy-efficient torque vectoring.

In the available studies, there is a general lack of explanation on how the vehicle-level targets have been initially defined, while considering actuator and tyre limits. The applications are usually presented without motivating the selected vehicle architecture or mentioning the achievable performance range. This topic is especially important in the early stages of vehicle development, for effective design of the hardware and control software. In fact, active chassis systems are usually conceived in several steps, following a V-cycle approach [22], starting from a simulation phase. The initial simulations involve the study of the performance envelope, i.e. the feasibility region, of the selected actuation system, and the evaluation of whether it meets the vehicle dynamics requirements. Such analysis is a prerequisite for developing the control strategies and testing them on dedicated virtual and physical prototype vehicles. The virtual phase contributes to limiting development costs from the proof-of-concept phase up to the pre-production phase and can include model-in-the-loop, hardware-in-the-loop, and driver-in-the-loop implementations. In terms of simulation methodologies for early analysis, relevant examples are: i) the objective assessment of the dynamic stabilisation capability of RWS and torque vectoring in [4], based on a phase-plane representation; and ii) the comparison [15] of the achievable understeer characteristics through torque vectoring, RMD, RWS, and the respective actuation combinations, by means of a high-fidelity model, which also defines the associated energy saving potential, although the vehicle dynamics performance indicators are neglected.

The common practice among the manufacturers of high-performance cars is to use multiple modelling approaches within the same model-in-the-loop setup, to capture the desired dynamics with the minimum computational burden and vehicle parameter set,

and then to adopt driving simulators to verify performance in scenarios that cannot be adequately evaluated through simulation alone. Accurate dynamic models with low computational cost and limited datasets are crucial for the timely computation of the key performance indicators (KPIs) of the lateral dynamics attribute, e.g. see the model comparisons in [22] and [23], where the latter neglects the suspension kinematics and compliance effects, and both do not embed an objective assessment based on a detailed set of industrially relevant KPIs. High-fidelity models, e.g. VI-CarRealTime by VI-grade, are widely employed for vehicle dynamics analyses, despite their relatively high computational cost. However, the use of advanced vehicle models in the early design stages poses challenges in terms of lack of available data, and engineering time to set up a realistic model parametrisation. In these phases, it is useful to adopt models that are as simple as possible, yet capable of generating realistic results in terms of achievable cornering response in steady-state and transient conditions, through KPIs. Unfortunately, the literature lacks a quantitative analysis of the accuracy level of the results associated with the specific features of simplified vehicle models.

This paper targets the identified gap by comparing vehicle dynamics models with increasing levels of complexity, and contrasting them with a VI-CarRealTime model. The focus is on using the simplified models in the early stages of a proof-of-concept, where feasibility studies of the chassis actuator suites are conducted to evaluate the respective performance range. The preliminary results can be refined with more complex models and complete datasets, once the targets for each chassis actuation system and vehicle parameters have been defined. The case study is a high-performance passenger car to be equipped with AC, RWS, or RMD. The novel contributions are:

- The assessment of the minimum level of modelling complexity to analyse the feasibility region and transient behaviour associated with active systems for lateral vehicle dynamics control.
- The quantitative analysis of the potential effects of FAC, RAC, RWS and RMD on the handling performance of the target vehicle in quasi-steady-state and transient conditions.

The remainder is structured as follows. Section 2 presents the considered simplified models with increasing levels of complexity, which are compared in Section 3, through a set of KPIs, with a benchmarking high-fidelity model in VI-CarRealTime. The most effective simplified model is identified and used in Section 4 to discuss the feasibility regions of FAC, RAC, RWS, and RMD in pure cornering conditions. Within the identified regions, Section 5 provides an example of proof-of-concept comparison of multiple actuation methods and initial decision-making, based on transient behaviour KPIs. Finally, the main conclusions are summarised in Section 6.

2. Vehicle dynamics models for handling evaluation

The objective is to assess the minimum level of modelling complexity for the initial handling performance evaluation of a high-performance car, without requiring a detailed set of vehicle parameters. A simplified model facilitates the feasibility region analysis and allows

an understanding of the potential benefit of a specific active system. More complex models should be used for a refinement of the targets, after the completion of the preliminary concept phase.

Four lateral dynamics models with increasing complexity are compared to a reference model of a McLaren 570s prototype, based on VI-CarRealTime, already validated against experimental data, see [24]. VI-CarRealTime contains a four-wheeled vehicle model considering the dynamics of the vehicle chassis (sprung mass) and four unsprung masses, for a total number of 14 degrees of freedom (DoFs), 6 of which are associated with the chassis and 2 with each unsprung mass (suspension displacement and wheel rotation). The steering and suspension system model uses a functional approach based on nonlinear maps describing the relevant properties, including kinematics and compliance aspects. Similarly, the other vehicle systems (e.g. the friction brakes and powertrain with open differential) are described by appropriate maps and algebraic equations. The simulation environment uses the Pacejka Magic Formula (version 5.2, [25]) tyre model formulation, considering combined forces/moments and relaxation dynamics.

All the simplified models are developed in Matlab/Simulink, based on the following assumptions:

- The longitudinal dynamics are decoupled from the lateral dynamics, to focus on the cornering response. Thus, the vehicle speed is considered a constant input, while the tyre slip ratios are assumed to be negligible. This can be a significant simplification, since the effect of traction can be relevant at high lateral acceleration values, at which the inner wheel normal load is the subject of a considerable reduction. The reader should refer to [26] and [27] for a comprehensive analysis of the effect of the longitudinal tyre forces – and their distribution between the front and rear axles – on the vehicle yaw moment and cornering response.
- The static suspension setup, including the static camber and toe angles, is the same for all models.
- The rear tyres have larger width and higher performance characteristics than the front ones, which brings a naturally understeering behaviour [26].

2.1. Single-track model with linearised lateral axle forces

The single-track model is widely used as reference model in control strategies, and as an internal model in sideslip angle estimators. The model combines the two wheels of each axle into an equivalent one, see Figure 1a, which highlights the main variables. The implemented model has linearised lateral axle forces as functions of slip angle and is referred to as LST in the remainder. The nonlinear motion equations are:

$$\begin{cases} mV(\dot{\beta} + \dot{\psi}) = F_{y,F}\cos\delta_{w,F} + F_{y,R}\cos\delta_{w,R} \\ J_z\ddot{\psi} = aF_{y,F}\cos\delta_{w,F} - bF_{y,R}\cos\delta_{w,R} \end{cases} \tag{1}$$

where V, $\dot{\psi}$ and $\dot{\beta}$ are the vehicle speed, yaw rate, and sideslip rate; m and J_z are the vehicle mass and yaw mass moment of inertia; a and b are the front and rear semi-wheelbases; and $F_{y,F}$ and $F_{y,R}$ are the front and rear lateral axle forces, expressed as a function of the actual

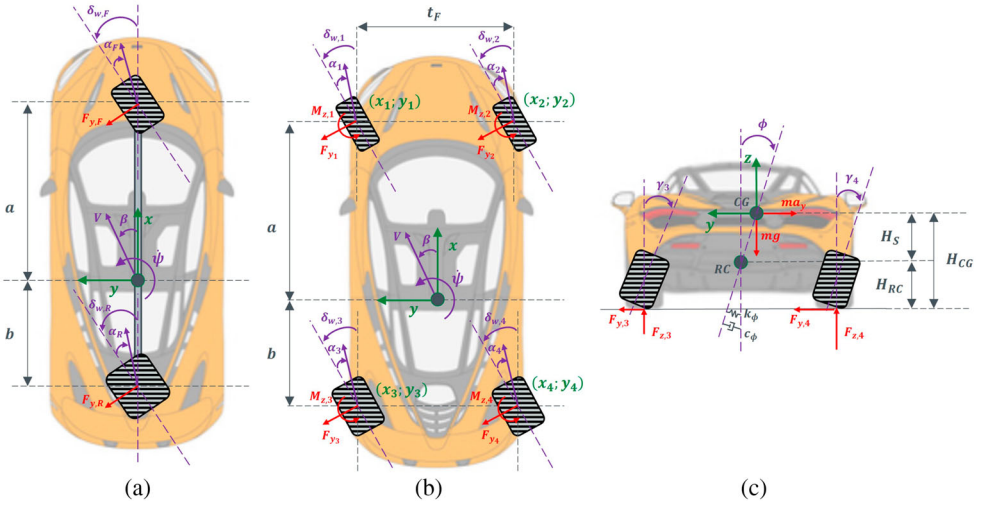

Figure 1. Schematic views of the considered vehicle dynamics models, with the definition of the main variables and parameters: (a) top view of the single-track model, (b) top view of the two-track model and (c) rear view of the roll dynamics model.

slip angles $\alpha_{act,i}$, where the subscript $i = F, R$ indicates the front or rear axles:

$$F_{y,F} = K_{y,F}\alpha_{act,F} \quad F_{y,R} = K_{y,R}\alpha_{act,R} \tag{2}$$

with $K_{y,i}$ being the axle cornering stiffness.

The actual slip angles are computed from the theoretical slip angles α_i:

$$\alpha_F = \delta_{w,F} - \beta - \frac{\dot{\psi}a}{V}; \quad \alpha_R = \delta_{w,R} - \beta + \frac{\dot{\psi}b}{V}, \text{with}$$
$$\delta_{w,F} = 0.5(\delta_{w,1}(\delta_{SW}) + \delta_{w,2}(\delta_{SW}) + \delta^0_{w,1} + \delta^0_{w,2}); \quad \delta_{w,R} = 0.5(\delta^0_{w,3} + \delta^0_{w,4}) \tag{3}$$

where $\delta_{w,F}$ and $\delta_{w,R}$ are the front and rear axle steering angles; $\delta_{w,1}$ and $\delta_{w,2}$ are the individual front wheel-steering angles, expressed as functions of the steering wheel angle, δ_{SW}, based on the steering system kinematics; and the notation $\delta^0_{w,j}$ indicates the static toe angles, with $j = 1, \ldots, 4$ referring to the relevant corners. The α_i values are subject to first-order dynamics [25], in the form of a filter with a time constant depending on the vehicle speed and tyre relaxation length, $L_{w,i}$:

$$L_{w,i} = \lambda_{F_{z0},i}\lambda_{SGAL,i}PTY1_i R_{0,i} \sin[2\tan^{-1}(\lambda_{F_{z0}}F_{z,i}PTY2_i(1 - PKY3_i|\gamma_i^0|))] \tag{4}$$

where $\lambda_{F_{z0},i}$, $\lambda_{SGAL,i}$, $PTY1_i$, $PTY2_i$ and $R_{0,i}$ are characteristic Pacejka (version 5.2, [25]) parameters, made available by the tyre supplier; $F_{z,j}$ is the vertical tyre load, considered constant in this model formulation, and γ_j^0 is the static camber angle.

$K_{y,i}$ is equal to the sum of the cornering stiffness values, $K_{y,j}$, of the two tyres on the same axle:

$$K_{y,F} = K_{y,1}(F_{z,1}, \gamma_1^0) + K_{y,2}(F_{z,2}, \gamma_2^0)$$

$$K_{y,R} = K_{y,3}(F_{z,3}, \gamma_3^0) + K_{y,4}(F_{z,4}, \gamma_4^0) \tag{5}$$

$K_{y,j}$ is obtained through the Pacejka 5.2 formulation [25], as a function of F_{z_j} and γ_j^0:

$$K_{y,j} = \lambda_{K_{y,j}} \lambda_{F_{z0,j}} F_{z0,j} PKY1_j (1 - PKY3_j |\gamma_j^0|) \sin\left[2\tan^{-1}\left(\frac{F_{z,j}}{\lambda_{F_{z0,j}} F_{z0,j} PKY2_j}\right)\right] \tag{6}$$

where $\lambda_{K_{y,j}}$, $\lambda_{F_{z0,j}}$, $F_{z0,j}$, $PKY1_j$, $PKY2_j$ and $PKY3_j$ are constant coefficients. The selected routine for obtaining the cornering stiffness purposely neglects the effect of the lateral load transfer as well as suspension kinematics and compliance, which is usually derived from vehicle experiments or simulations based on higher fidelity models, e.g. see [25]. In fact, the purpose of the analysis is to show the achievable accuracy level of models targeting the earliest vehicle design stages, when a physical prototype or a reliable multi-body/high-fidelity model do not exist yet. Also, if realistic suspension kinematics and compliance characteristics are already available in the initial development phases, it is more practical to associate them directly with a nonlinear tyre model, which will be shown in the following sections, rather than with the equivalent linearised lateral axle force model of the LST formulation.

$F_{z,j}$ includes the static load and aerodynamic downforce contributions, which are equally split between the wheels of each axle, according to the single-track model approach:

$$F_{z,1} = F_{z,2} = \frac{1}{2}\left(mg\frac{b}{L} + C_{Down,F}V^2\right); \quad F_{z,3} = F_{z,4} = \frac{1}{2}\left(mg\frac{a}{L} + C_{Down,R}V^2\right) \tag{7}$$

where g is the gravitational acceleration; and $C_{Down,i}$ is the aerodynamic downforce coefficient of the axle.

2.2. Single-track model with nonlinear lateral axle forces

The dynamics of this model, referred to as NLST in the remainder, are expressed by Eq. (1), where the lateral axle forces are computed as the sum of the respective lateral tyre forces, $F_{y,j}$:

$$\begin{aligned} F_{y,F} &= F_{y,1}(F_{z,1}, \alpha_F, \gamma_1^0) + F_{y,2}(F_{z,2}, \alpha_F, \gamma_2^0) \\ F_{y,R} &= F_{y,3}(F_{z,3}, \alpha_R, \gamma_3^0) + F_{y,4}(F_{z,4}, \alpha_R, \gamma_4^0) \end{aligned} \tag{8}$$

with $F_{y,j}$ being calculated through version 5.2 of the Pacejka model. The single-track assumption refers to the fact that the lateral load transfers are neglected in the computation of $F_{y,j}$, i.e. $F_{z,1} = F_{z,2}$ and $F_{z,3} = F_{z,4}$. Similarly to the discussion in Section 2.1, reference [25] presents a methodology to obtain the lateral axle force characteristic for a single-track model, starting from high-fidelity model simulations or vehicle experiments, which, however, is not practical for the initial decision-making phases, because of the lack of model parameters or a vehicle prototype.

2.3. Nonlinear two-track model

The nonlinear two-track (NLTT) model (Figure 1b) is based on the following lateral force and yaw moment balance equations:

$$\begin{cases} mV(\dot{\beta}+\dot{\psi}) = \sum_{j=1}^{4} F_{y,j}\cos\delta_{w,j} \\ J_z\ddot{\psi} = \sum_{j=1}^{4} F_{y,j}x_j\cos\delta_{w,j} + \sum_{j=1}^{4} F_{y,j}y_j\sin\delta_{w,j} \end{cases} \tag{9}$$

where x_j and y_j are the longitudinal and lateral coordinates of the wheel corners.

The vertical tyre loads include the lateral load transfers, $\Delta F_{z,i}$:

$$\begin{aligned} F_{z,1} &= \frac{1}{2}\left(mg\frac{b}{L} + C_{Down,F}V^2\right) - \Delta F_{z,F}; \quad F_{z,2} = \frac{1}{2}\left(mg\frac{b}{L} + C_{Down,F}V^2\right) + \Delta F_{z,F} \\ F_{z,3} &= \frac{1}{2}\left(mg\frac{a}{L} + C_{Down,F}V^2\right) - \Delta F_{z,R}; \quad F_{z,4} = \frac{1}{2}\left(mg\frac{a}{L} + C_{Down,\mathrm{R}}V^2\right) + \Delta F_{z,R} \end{aligned} \tag{10}$$

where the $\Delta F_{z,i}$ terms are expressed as functions of the lateral acceleration $V(\dot{\beta}+\dot{\psi})$, through the moment balance equations about the roll centres, by considering a fixed value, k_F, of the front-to-total roll moment distribution:

$$\begin{aligned} \Delta F_{z,F} &= \frac{1}{t_F}\left[mV(\dot{\beta}+\dot{\psi})\left(\frac{bH_{RC,F}}{L} + k_F H_s\right)\right] \\ \Delta F_{z,R} &= \frac{1}{t_R}\left[mV(\dot{\beta}+\dot{\psi})\left(\frac{aH_{RC,R}}{L} + (1-k_F)H_s\right)\right] \end{aligned} \tag{11}$$

where $H_{RC,i}$ is the roll centre height of the considered suspension; H_s is the distance between the centre of gravity and the roll centre, see Figure 1c; and t_i is the track width of the considered axle.

Also in this formulation, each tyre is modelled through the version 5.2 of the magic formula, according to which the static camber and toe angles as well as the vertical tyre load affect the individual lateral forces.

2.4. Nonlinear two-track model with body roll dynamics and suspension elasto-kinematics

This model, referred to as nonlinear two-track model including body roll, suspension kinematics and elasto-kinematics (NLTTEK), accounts also for the roll dynamics, which have a direct effect on the wheel positioning w.r.t. the road [28]. Its force and moment balance

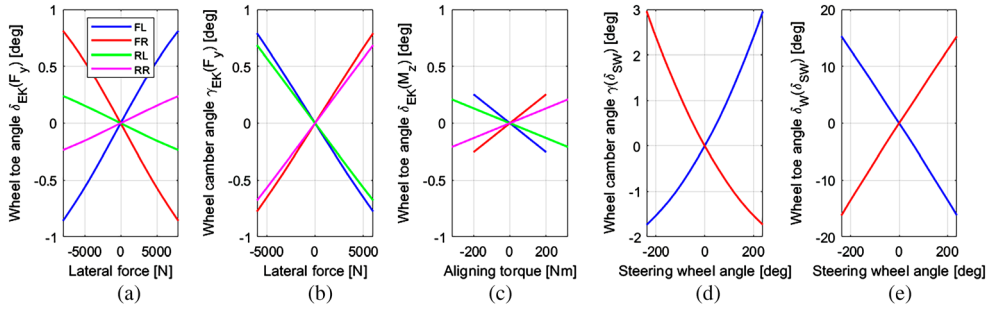

Figure 2. Compliance and kinematic characteristics implemented in the NLTTEK model: (a) toe angle as a function of lateral force, (b) camber angle as a function of lateral force, (c) toe angle as a function of aligning torque, (d) camber angle as a function of steering wheel angle and (e) toe angle as a function of steering wheel angle. The sign conventions are the same as in ref. [28], i.e. positive camber corresponds to a wheel in a top-out configuration, and a positive toe angle corresponds to toe-in.

equations are:

$$\begin{cases} mV(\dot{\beta}+\dot{\psi}) = \sum_{j=1}^{4} F_{y,j}\cos\delta_{w,j} \\ J_z\ddot{\psi} = \sum_{j=1}^{4} F_{y,j}x_j\cos\delta_{w,j} + \sum_{j=1}^{4} F_{y,j}y_j\sin\delta_{w,j} + \sum_{j=1}^{4} M_{z,j} \\ (J_x + mH_s^2)\,\ddot{\phi} = mH_sV(\dot{\beta}+\dot{\psi}) - C_\phi\dot{\phi} - K_\phi\phi + mgH_s\phi \end{cases} \tag{12}$$

where ϕ (see Figure 1c) is the roll angle; $M_{z,j}$ is the self-aligning moment of the respective tyre; J_x and J_y are the roll and pitch moments of inertia; m_s is the sprung mass; K_ϕ is the total suspension roll stiffness, given by the sum of the front and rear roll stiffness values, i.e. $K_\phi = K_{\phi,F} + K_{\phi,R}$; and $C_\phi = C_{\phi,F} + C_{\phi,R}$ is the equivalent total suspension roll damping coefficient.

The theoretical steering angles $\delta_{w,j}$ and camber angles γ_j, before the filtering related to tyre relaxation, are expressed as nonlinear functions (see the example in Figure 2) of the steering wheel angle, δ_{SW}, lateral tyre forces, $F_{y,j}$, and tyre self-aligning torques, $M_{z,j}$, according to the approach in [29]:

$$\begin{aligned} \delta_{w,j} &= \delta_{w,j}^0 + \delta_{w,j}(\delta_{SW}) + \delta_{EK,j}(F_{y,i}) + \delta_{EK,j}(M_{z,j}) \\ \gamma_j &= \gamma_j^{\,0} + \gamma_j(\delta_{SW}) + \gamma_{EK,j}(F_{y,i}) \end{aligned} \tag{13}$$

where the subscripts 'EK' in the notations indicate the elasto-kinematics-related contributions.

The dependency on the suspension jounce is not considered, since the suspension deformation is not modelled, to keep the number of DoFs as low as possible. The vehicle body roll angle and wheel camber angles due to the suspension elasto-kinematics facilitate the accurate calculation of the inclination angle $\gamma_{I,j}$, which is the input for the lateral forces in the Pacejka model. In the NLTTEK model, the camber angle γ_j is defined as the relative angle w.r.t. to the originally vertical axis of the vehicle body in zero roll angle conditions. Such reference axis varies its orientation with the roll motion. Therefore, the

value of the inclination angle, $\gamma_{I,j}$, defined as the angle between the wheel centre plane and the normal to the road plane, is equal to the algebraic sum of the previously defined wheel camber angle and the body roll angle, under the simplifying assumption of zero suspension-kinematics-based roll angle compensation in cornering.

The lateral load transfers are expressed as the sum of a contribution related to the lateral acceleration, and a contribution proportional to the roll angle and roll rate:

$$\Delta F_{z,F} = \frac{1}{t_F}\left[\frac{mV(\dot{\beta}+\dot{\psi})bH_{RC,F}}{L} + K_{\phi,F}\phi + C_{\phi,F}\,\dot{\phi}\right]$$
$$\Delta F_{z,R} = \frac{1}{t_R}\left[\frac{mV(\dot{\beta}+\dot{\psi})aH_{RC,R}}{L} + K_{\phi,R}\phi + C_{\phi,R}\,\dot{\phi}\right] \tag{14}$$

3. Model comparison based on lateral dynamics indicators

This section evaluates the accuracy of the models in Section 2 through a comparison with the reference model in VI-CarRealTime. The assessment is based on objective KPIs, which are computed along the following three open-loop ISO manoeuvres, covering the quasi-steady-state and transient cornering response: i) the steering pad at constant speed test (SPCS), [30]; ii) the step input steering manoeuvre (SI), [31]; and iii) the sine-sweep input test with linearly increasing frequency (SSI), [31].

3.1. Steering pad at constant speed results

The SPCS manoeuvre [22,30] characterises the full lateral acceleration range of the cornering response, in quasi-steady-state conditions. A constant test speed of 100 km/h is maintained while gradually increasing the steering wheel angle, δ_{SW}, from 0 to 180 deg, with a rate of 10 deg/s. The data collected during the SPCS manoeuvre is typically expressed as a function of the lateral acceleration. The understeer curve describes the relationship between δ_{SW} and the lateral acceleration, a_y, expressed in g. This curve represents the relative lateral slip behaviour between the front and rear axles, and is always paired with the sideslip angle curve as a function of a_y, which characterises the rear axle behaviour, and thus relates to vehicle stability.

The list of the dedicated SPCS KPIs [1,12,30,32], is provided in Table 1 and shown in Figure 3a, while the values for the considered models are reported in Figure 4. With increasing model complexity, the performance difference w.r.t. the reference VI-CarRealTime model decreases in both the linear and nonlinear regions, see Figure 4a and Figure 4b. The LST and NLST models share the same steering wheel angle gradient [31,32], K_{a_y}, which indicates the vehicle agility level in terms of vehicle reactions to the steering input for low and medium lateral accelerations; their difference lies in the nonlinear part of the front and rear axle characteristics. The lateral load transfer, captured in the NLTT model, contributes to a marginal reduction in K_{a_y}, due to the influence of the vertical loads on the cornering stiffness of the individual tyres. In the NLTTEK model, the kinematic and compliance effects influence the level of understeer through the recovery of camber angle during steering, and the toe angle variations associated with the lateral forces and aligning moments. These effects are more pronounced than the camber loss under lateral force. The difference in K_{a_y} between the VI-CarRealTime and NLTTEK models, 55.7 deg/g against 53.6 deg/g,

Table 1. KPIs for each of the selected ISO tests.

KPIs	Units	Test	Description
K_{a_y}	deg/g	SPCS	Steering wheel angle gradient w.r.t. lateral acceleration
$a_{y,EoL}$	g	SPCS	End of the linear region of the understeer curve (computed based on a minimum deviation level from a linearity condition defined from 0.2 g to 0.4 g)
$a_{y,85\%max}$	g	SPCS	85% of the maximum lateral acceleration
$a_{y,max}$	g	SPCS	Maximum lateral acceleration
$\delta_{SW}@a_{y,max}$	deg	SPCS	Steering wheel angle at the maximum lateral acceleration
$K_{a_{y,85\%max}}$	deg/g	SPCS	Steering wheel angle gradient evaluated at $a_{y,85\%max}$
K_β	deg/g	SPCS	Sideslip gradient w.r.t. lateral acceleration
$\lvert\beta_{EoL}\rvert$	deg	SPCS	End of the linear region of the sideslip curve as a function of lateral acceleration
$\lvert\beta_{max}\rvert$	deg	SPCS, SI	Maximum sideslip angle
$\dot{\psi}_{RT}$	ms	SI	Yaw rate rise time
$\dot{\psi}_{ST}$	ms	SI	Yaw rate settling time
$\dot{\psi}_{OS}$	%	SI	Yaw rate overshoot
$\dot{\psi}_{PT}$	ms	SI	Yaw rate peak time
β_{ST}	ms	SI	Sideslip angle settling time
$\lvert\dot{\beta}_{max}\rvert$	deg/s	SI	Maximum sideslip rate
$A_{\dot{\psi}} = G_{\dot{\psi}max}/G_{\dot{\psi}0}$	–	SSI	Dynamic yaw rate enlargement, i.e. the ratio between the maximum response magnitude and the steady-state response magnitude
$f_{G_{\dot{\psi}max}}$	Hz	SSI	Frequency corresponding to the maximum yaw rate response magnitude
$\Delta t_{0.5\dot{\psi}}$	ms	SSI	Yaw rate time delay @0.5 Hz
$\Delta t_{1\dot{\psi}}$	ms	SSI	Yaw rate time delay @1 Hz
$\Delta t_{0.5a_y}$	ms	SSI	Lateral acceleration time delay @0.5 Hz
Δt_{1a_y}	ms	SSI	Lateral acceleration time delay @1 Hz
$\Phi_{1\beta}$	deg	SSI	Sideslip angle phase @1 Hz
$A_\beta = G_{\beta max}/G_{\beta 0}$	-	SSI	Dynamic sideslip angle enlargement

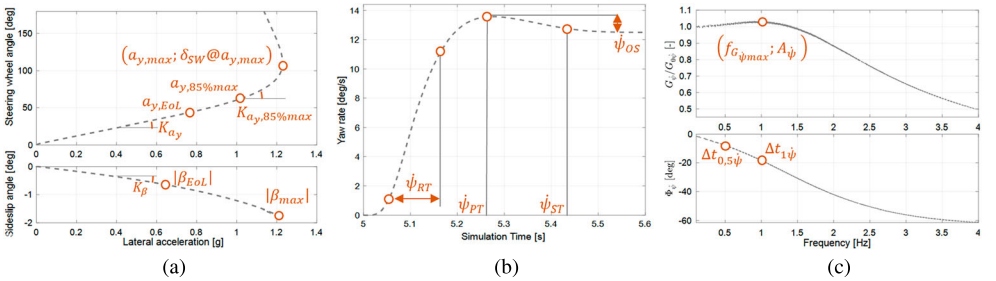

Figure 3. Overview of the KPIs for each of the selected ISO tests: (a) SPCS, (b) SI and (c) SSI.

is mainly caused by the absence in the NLTTEK implementation of the whole set of camber and toe angle contributions linked to the suspension kinematics.

$a_{y,EoL}$ is the parameter describing the end of the linear range of the understeer characteristic. A relatively large $a_{y,EoL}$ provides the driver with the perception of a better performing and consistently responsive, controllable and predictable vehicle, although the presence of

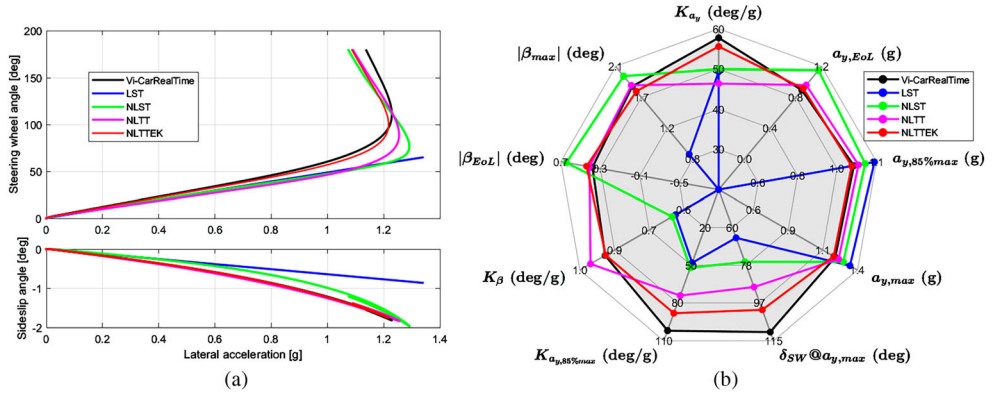

Figure 4. SPCS results plots for model comparison: (a) understeer and sideslip curves and (b) corresponding KPIs in a spider chart.

some form of nonlinearity would be beneficial to warn the driver that he/she is approaching the cornering limit. The extension of the linear steering response region can also be achieved through static setup adjustments, i.e. without additional active systems. However, the passive adjustments could lead to unstable behaviour in transients, which is not the case when the $a_{y,EoL}$ increase is implemented through active methods. $a_{y,EoL}$ cannot be calculated for the LST model, since its understeer characteristic is entirely linear. Factors such as the load transfers and the toe and camber angles play a vital role in determining the $a_{y,EoL}$ position on the characteristic curve. In NLST, $a_{y,EoL}$ is ~ 1.2 g, quite close to the maximum lateral acceleration, $a_{y,max}$, of 1.3 g. For NLTT and NLTTEK, the transition into the nonlinear zone is smoother, and $a_{y,EoL}$ decreases as soon as the elasto-kinematics and lateral load transfer contributions become significant.

$a_{y,max}$, $a_{y,85\%max}$, $K_{a_{y,85\%max}}$, and $\delta_{SW}@a_{y,max}$ describe the shape of the nonlinear region of the understeer characteristic. More specifically, $a_{y,max}$ is important to evaluate the grip level on the front axle, since it is the first one to saturate; $a_{y,85\%max}$ and $K_{a_{y,85\%max}}$ give an indication of the vehicle agility level in terms of reactions to steering inputs at high lateral accelerations, and $\delta_{SW}@a_{y,max}$, in conjunction with the K_{a_y} value in the linear region, highlights the potential magnitude of the nonlinearity of the vehicle behaviour perceived by the driver, and the average steering wheel angle amplitude required during limit cornering. From the spider chart in Figure 4b, also in this case NLTTEK is the model that comes the closest to the reference one. The difference between NLTTEK and the VI-CarRealTime model is primarily due to the load transfer computation, since in the high-fidelity model the roll centre heights, track widths and roll stiffness of front and rear axles vary according to the suspension elasto-kinematics, whereas these parameters are all considered constant in NLTTEK. The calculation of the lateral load transfer based on roll angle (NLTTEK) rather than only the lateral acceleration (NLTT) significantly improves the accuracy.

W.r.t. the sideslip curve, the evaluated KPIs are similar to those for the steering wheel angle curve: K_β, which relates to the driver's perception of a disconnection between the front and rear axle responses, and indicates whether the front axle is over- or under-reactive, to objectivise the impression of compactness and driving precision; and $|\beta_{EoL}|$, which, along with $|\beta_{max}|$, indicates how much the vehicle tends to close the trajectory at

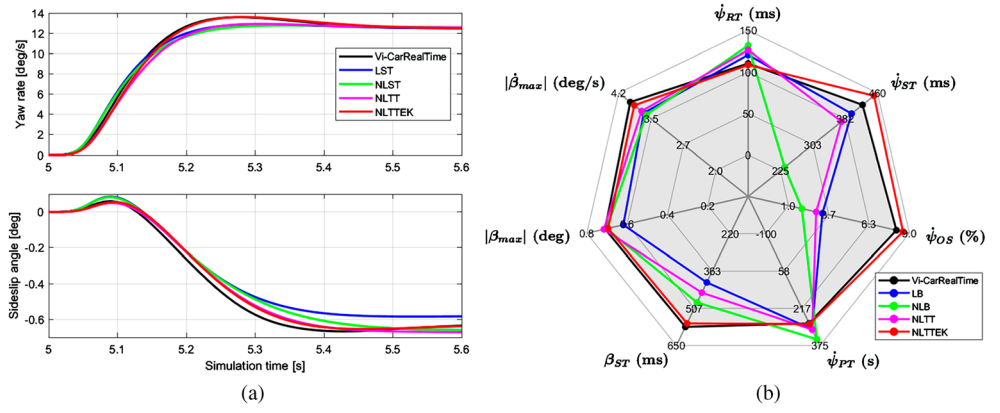

Figure 5. SI results for model comparison: (a) time profiles of yaw rate and sideslip angle and (b) corresponding KPIs in a spider chart.

the cornering limit, and can correlate with the driver's perception of understeer or oversteer. The general goal is to prevent abrupt changes in the sideslip gradient, since, when this rises too quickly, the driver will have the undesirable feeling of a 'snap oversteer' condition [12]. As highlighted by Figure 4a and the KPIs, the four-contact models better capture the quasi-steady-state sideslip angle response.

3.2. Step input results

The main aim is to assess the vehicle transient response in the time domain. The steering input is swiftly applied according to the ISO standard [31], until the steering wheel angle corresponding to a specific lateral acceleration target is reached. In this instance, the speed is set to 100 km/h, and the target acceleration is 0.6 g. Due to the steering wheel angle gradient difference, each model has different steering targets.

Figure 5 reports the yaw rate and sideslip angle time responses, as well as the values of the KPIs defined in Table 1, and shown in Figure 3b, see also the discussion on the manoeuvre in [33]. The yaw rate rise time, $\dot{\psi}_{RT}$, and settling time, $\dot{\psi}_{ST}$, are significantly influenced by the accuracy of the lateral load transfer model, and they respectively give an indication on the agility and stability level of the vehicle. Indeed, NLTTEK comes the closest to VI-CarRealTime. In NLTTEK, the vertical loads directly and realistically impact the computation of the tyre relaxation lengths, providing the response dynamics of the lateral forces. The roll degree of freedom and the consideration of compliances contribute to the reduction of the yaw damping of the system, see the difference in the overshoot values, $\dot{\psi}_{OS}$, which, along with $\dot{\psi}_{PT}$, is an indicator of vehicle stability (or its lack). The effect of $M_{z,j}$ is an increase in the settling time immediately after the step. From the analysis of the sideslip dynamics, corresponding to $|\beta_{max}|$ and $|\dot{\beta}_{max}|$, which are related to agility evaluation and cornering performance, it is evident how the inclusion of non-linearities affects the rear axle response.

3.3. Sine-sweep input results

The SSI manoeuvre consists of a steering input with constant amplitude $\delta_{SW,max}$ and linearly increasing frequency, from 0.05 to 4 Hz, see [31], at a constant vehicle speed of

100 km/h. This procedure enables to evaluate the phase lags and dynamic overshoot of the response. $\delta_{SW,max}$ is selected based on the SPCS results, where the target lateral acceleration is $a_y = 4\,\mathrm{m/s^2}$. Thus, the steering input is limited to the linear range relevant to the frequency domain analysis.

The evaluation process follows the approach in [34], according to which equivalent transfer functions are obtained from the discrete fast Fourier transform of the input x, namely δ_{SW}, and the outputs y, specifically $\dot{\psi}$, a_y, and β. The result, indicated as H and including the dependency on the frequency f, is used to evaluate the auto spectrum S_{xx}, and the cross-spectrum S_{yx}. In particular, the auto spectrum is calculated by multiplying the discrete fast Fourier transform of the input, H_x, by its complex and conjugate, H_x^*:

$$S_{xx}(f) = H_x(f)\, H_x^*(f) \tag{15}$$

The cross-spectrum is computed by multiplying the discrete fast Fourier transform of the output signal, H_y, by H_x^*:

$$S_{yx}(f) = H_y(f)\, H_x^*(f) \tag{16}$$

The transfer function is then given by:

$$G_y(f) = \frac{S_{yx}(f)}{S_{xx}(f)} \tag{17}$$

This analysis considers the steering wheel angle to yaw rate, lateral acceleration, and sideslip angle transfer functions:

$$G_{\dot{\psi}}(f) = \frac{S_{\dot{\psi}\delta_{SW}}(f)}{S_{\delta_{SW}\delta_{SW}}(f)}; \quad G_{a_y} = \frac{S_{a_y\delta_{SW}}(f)}{S_{\delta_{SW}\delta_{SW}}(f)}; \quad G_\beta = \frac{S_{\beta\delta_{SW}}(f)}{S_{\delta_{SW}\delta_{SW}}(f)} \tag{18}$$

The comparison of the frequency response behaviour of the different modelling approaches is based on the yaw rate frequency response, given by $G_{\dot{\psi}}$, and the spider chart summarising the SSI KPIs, see Figure 6a and Figure 6b. The models have different understeer gradients; therefore, the steering input required to achieve a lateral acceleration of $4\,\mathrm{m/s^2}$ is not the same. Hence, the amplitude of $G_{\dot{\psi}}$ is divided by the static gain, $G_{\dot{\psi}0}$. As the models share the same vehicle mass and yaw mass moment of inertia, the differences are primarily caused by the lateral load transfer effect on the tyre cornering stiffness and relaxation length. Indeed, a change in cornering stiffness of the axles leads to variations in bandwidth and eigenfrequency, while a change in relaxation length has an impact on both the peak and delay of the response. These effects are caught by the yaw dynamics enlargement, $A_{\dot{\psi}}$, and the frequency value corresponding to the maximum response, $f_{G_{\dot{\psi}max}}$. These two KPIs, along with $\phi_{1\beta}$ and A_β, indicate the possibility of the driver to obtain very different and potentially unexpected vehicle responses, depending on the excitation frequency. The models neglecting the roll dynamics have the same value of $A_{\dot{\psi}}$, and respond almost identically up to a frequency of 1 Hz, while NLTTEK has an enlargement value of 1.07, compared to 1.03 of VI-CarRealTime. The yaw damping value tends to decrease as the complexity of the models increases. However, such decrease is more evident in NLTTEK than in VI-CarRealTime, because in the former the roll dynamics are simulated with constant roll stiffness and, more importantly, roll damping, differently from the high-fidelity model case, where they vary

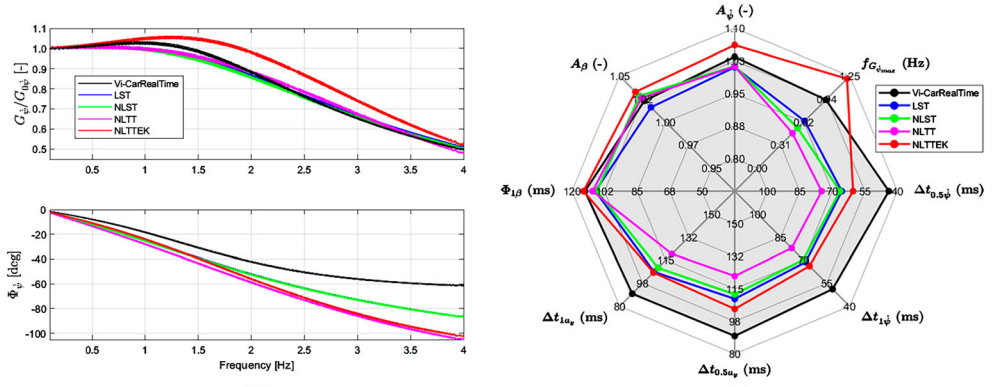

Figure 6. SSI results for model comparison: (a) yaw rate frequency response and (b) corresponding KPIs in a spider chart.

depending on the vertical displacement and its rate at the individual corners, and directly affect the load transfers. The previously mentioned differences between the models are also highlighted by $\Delta t_{0.5\dot{\psi}}$, $\Delta t_{1\dot{\psi}}$, $\Delta t_{0.5a_y}$, and Δt_{1a_y}. The combination of such KPIs provides information on the time response at various frequencies to the driver steering input, and more specifically on the varying time response and delay between the front and rear axles, where the yaw rate indicators relate to the front axle response, while the lateral acceleration ones to the rear axle response. Hence, these indexes also reflect the sense of agility and connection between the steering wheel and the road.

3.4. Model comparison outcomes

The previous discussion has highlighted that, among the simplified models, NLTTEK brings minimal differences in the relevant SPCS- and SI-oriented KPIs w.r.t. VI-CarRealTime, and in the SSI test the two models are in good agreement up to a steering input frequency of ~ 1 Hz. Therefore, NLTTEK can be used for initial feasibility studies to evaluate the vehicle operational range with the addition of an active system. In the next sections, the feasibility region analysis will be conducted through the NLTTEK model, by discussing the effect of front and rear AC, RWS, and RMD on the lateral dynamics KPIs in Table 1.

4. Active systems feasibility region analysis

4.1. Methodology

This section describes the procedure for evaluating the feasibility regions through the NLTTEK model. The process assesses the performance envelope that can be achieved w.r.t. the reference passive vehicle. The feasibility regions are obtained through the SPCS test, by considering fixed control actions corresponding to the minimum and maximum values for a single actuator, under the assumption, which was verified through simulations, of monotonically varying vehicle behaviour as a function of the selected control input. In this way,

Table 2. Actuation limits and control action nomenclature.

Actuator	Control action	Minimum	Maximum
FAC	$\gamma_{AC,1}$, $\gamma_{AC,2}$	−5 deg	5 deg
RAC	$\gamma_{AC,3}$, $\gamma_{AC,4}$	−5 deg	5 deg
RWS	$\delta_{RWS,3}$, $\delta_{RWS,4}$	−1 deg	1 deg
RMD	ϵ_{RMD}	25%	75%

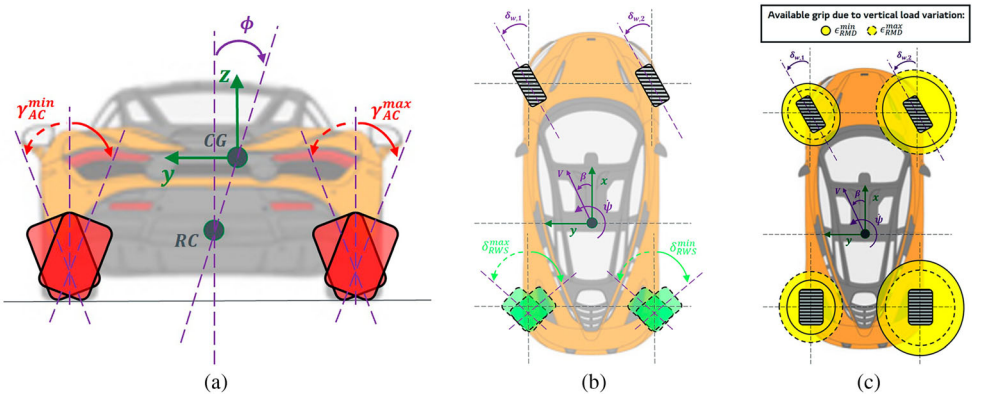

Figure 7. Schematic representation of the considered control actions: (a) variable RAC, (b) RWS and (c) RMD.

the locus of the achievable understeer and sideslip angle characteristics is obtained, providing an indication of their adjustability through active control. Table 2 reports the selected actuation ranges for front and rear AC, RWS, and RMD control, which are based on internal company investigations and know-how, accounting for currently available actuators as well as tyres. Since the specific tyres are characterised by very large cornering stiffness and much more limited camber stiffness, it has been decided to opt for a relatively large camber variation range and a small rear steering range, which is also consistent with the statements in [9] and [10].

Figure 7 illustrates the qualitative effect of the considered active systems. Evaluations of the required actuation power, energy consumption, design and packaging constraints, or actuator dynamics – unless otherwise specified – are outside the scope of this study.

The camber control action is designed as a deviation from the camber behaviour of the passive vehicle. Therefore, the AC control contribution, namely $\gamma_{AC,j}$, is algebraically added to the kinematic and compliance camber contributions:

$$\gamma_j = \gamma_j^{\,0} + \gamma_j(\delta_{SW}) + \gamma_{EK,j}(F_{y,j}) + \gamma_{AC,j} \tag{19}$$

The value of $\gamma_{AC,j}$ is the same for both wheels of the axle, i.e. one wheel is actuated towards a top-out condition, while the other one towards a top-in condition.

Similarly, with RWS, the rear steering angles are affected by an additional δ_{RWS} contribution, here reported for the rear left wheel:

$$\delta_{w,3} = \delta_{w,3}^{0} + \delta_{EK,3}(F_{y,3}) + \delta_{EK,3}(M_{z,3}) + \delta_{RWS} \tag{20}$$

The considered RWS range, corresponding to the same control action for the right and left rear wheels, is sufficient to significantly modify the magnitude of the rear lateral forces.

RMD control, implemented through active suspension actuators at the individual corners or active anti-roll bars, enables to continuously change the front-to-total anti-roll moment distribution. The control action, denoted as ϵ_{RMD}, is directly embedded in the NLTTEK lateral load transfer formulation, to partition the total roll stiffness among the axles:

$$\Delta F_{z,F} = \frac{1}{t_F}\left[\frac{mV(\dot{\beta}+\dot{\psi})bH_{RC,F}}{L} + \epsilon_{RMD}K_{\phi}\phi + C_{\phi,F}\dot{\phi}\right]$$
$$\Delta F_{z,R} = \frac{1}{t_R}\left[\frac{mV(\dot{\beta}+\dot{\psi})aH_{RC,R}}{L} + (1-\epsilon_{RMD})K_{\phi}\phi + C_{\phi,R}\dot{\phi}\right] \quad (21)$$

Given the inherently high roll stiffness – and thus very low roll angle values – of the specific vehicle, the RMD actuation is not used to reduce the magnitude of the vehicle roll motion, but only to vary the tyre load distribution. A different RMD formulation, e.g. see [4] would be used for conventional passenger cars, characterised by significantly higher amplitudes of the roll angle response.

4.2. Results

The feasibility regions for each actuator configuration are the coloured areas in Figure 8, whose boundaries correspond to the actuation limits in Table 2. Constant AC and RWS control inputs shift the understeer characteristic towards positive and negative lateral accelerations. The offsets arise from the inclination and steering angles generated by the control actions, which affect the lateral forces. This can also be observed in the sideslip angle characteristic, which, for the same reason, does not start from the origin. Figure 8 highlights that RWS can modify the steering wheel angle gradient, which is the case also for FAC and RAC, although in a much more limited manner. On the other hand, RMD has no impact in the linear region of the understeer characteristic, and its effect becomes evident for high lateral acceleration values, corresponding to significant lateral load transfers. Within the feasibility region of each actuator set, during the design phase it is possible to define achievable and desirable reference understeer characteristics, whose actuation levels can be deduced by interpolating the characteristics obtained for fixed and intermediate actuation efforts.

$a_{y,max}$ can be increased to a minimal extent with RAC and RWS, and more noticeably with FAC and RMD, up to approximately 1.3 and 1.24 g, respectively. Therefore, systems that implement control actions on the rear axle can only achieve marginal improvements in lateral acceleration. A significant increase in the $a_{y,max}$ performance can only be obtained through the combination of another system that also influences the front axle response. FAC brings a lateral acceleration increase through improved lateral grip utilisation, especially on the wheels with higher vertical loads, whilst RMD leverages the lateral load transfer distribution between the axles, thus enabling higher front lateral force by means of reduced front lateral load transfer. All areas in Figure 8 facilitate the development of a control strategy that can extend the linear zone of the understeer characteristic, and thus the value of $a_{y,EoL}$. This provides the driver with the impression of driving a better performing and consistently responsive vehicle.

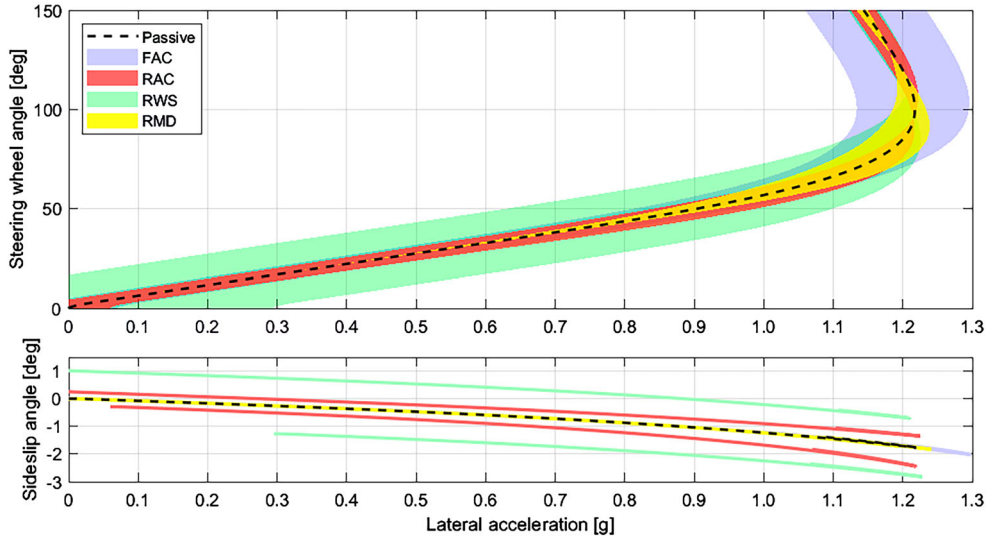

Figure 8. Feasibility regions for the FAC, RAC, RWS and RMD actuations, obtained with the SPCS test at 100 km/h.

The steering angle corresponding to the maximum lateral acceleration is of significant interest, since this indicator, evaluated together with the others, may be associated to the level of understeer perceived by the driver in the linear and nonlinear regions. For example, with FAC, the value remains approximately the same (100 deg) across the control action range. The boundaries of the feasible FAC region also highlight a modification in the shape of the understeer characteristic. This behaviour does not occur for the other systems because $\delta_{SW}@a_{y,max}$ shifts to higher or lower values, depending on the control action, w.r.t. the value for the passive vehicle. With RAC and RWS, the understeer curve does only shift vertically, while maintaining the same value of $a_{y,max}$.

Variable RMD, as well as FAC, have no effect on β_{EoL} and K_β, since the two systems primarily act on the front axle. Obviously, β_{max} changes because of the front axle saturation. RWS and RAC can shift the sideslip curve and enhance vehicle stability by reducing the sideslip angle at the expense of performance.

The simplicity and strength of the envelope approach lies in the lack of need for a control strategy for assessing the achievable performance range, as the control actions are constant values that do not depend on operating conditions or a specific reference. Obviously, non-zero lateral accelerations at zero steering wheel angle do not represent realistic solutions, but are useful to quantify the modifiability of the linear region of the understeer characteristic. In summary, the main benefits of the approach are:

1. Understanding in advance the targets that can be achieved with a specific chassis control system in terms of handling performance.
2. Defining a reference understeer characteristic that is compliant with the vehicle targets, and falls within the identified actuation limits, to be used for the following control algorithm development.

5. Case study

This section covers a case study in which the selection of an active system will be made based on the feasibility region analysis, and a set of vehicle-level handling targets. Obviously, the choices will depend on the specific requirements. Differently from the previous sections, the case study results consider the involved actuation rate saturations, as well as the bandwidth of potential actuators available in the market. Interestingly, it has been verified that the actuation dynamics constraints do not significantly affect the vehicle-level response along the considered manoeuvres.

In this illustrative example, the requirements that must be met are:

- Reducing K_{a_y} by at least 5% w.r.t. the passive vehicle;
- Keeping the same $a_{y,max}$ as for the passive vehicle;
- Increasing vehicle responsiveness by reducing $\dot{\psi}_{PT}$, $\dot{\psi}_{RT}$, and $\Delta t_{1_{\dot{\psi}}}$.

Such requirements are typical of a vehicle agility enhancement to be achieved through a sports-oriented driving mode, which allows drivers to gradually increase their engagement and confidence in their high-performance vehicle.

Among the considered active systems, RMD does not fulfil the target to reduce the understeer level in the linear region, see Section 4, and thus will not be included in the following discussion. The next step is to define the effort level of each actuator that allows the fulfilment of the requirements. In this illustrative example, the reference camber and rear steering angle profiles that are provided to the vehicle model are generated by look-up tables as functions of the steering wheel angle, δ_{SW}, for the given vehicle speed, V, to keep the same $a_{y,max}$ of the passive vehicle, and achieve the target K_{a_y} reduction. The actuation maps have been derived through interpolation of the control actions within the respective steady-state feasibility regions. The same look-up tables have been used for both the quasi-steady-state and transient tests.

Figure 9a includes the understeer characteristics for the controlled vehicle with FAC, RAC and RWS, and the passive vehicle. The controlled configurations achieve the two quasi-steady-state targets. In fact, Figure 9 highlights lower K_{a_y}, with different shapes in the transition from the linear to the nonlinear regions. FAC does not modify the β characteristic w.r.t. the passive vehicle, which – instead – is the case for RWS and RAC, for which K_β, β_{EoL}, and β_{max} increase by $\sim$40%. In general, the action of a single chassis actuation system cannot independently modify both the understeer and sideslip curves.

To meet the third set of requirements, the active systems, designed under quasi-steady-state conditions, are analysed in dynamic conditions along the SI and SSI tests, see Figure 10 and Figure 11. Differences w.r.t. the passive vehicle are visible in all KPIs in Figure 10, except for FAC, which has a dynamic response that is very close to that of the passive vehicle, apart from a reduction of $\dot{\psi}_{PT}$ and β_{ST}. RAC and RWS exhibit greater differences in terms of sideslip angle response. In fact, both β_{max} and $\dot{\beta}_{max}$ increase by $\sim$20% w.r.t. the passive case. In general, the presence of active systems enhances the reactivity both in terms of $\dot{\psi}$ and β, see the trends of $\dot{\psi}_{RT}$, β_{ST} and $\dot{\psi}_{PT}$. RWS much more significantly decreases the response time than the other systems, although this results in a substantial increase in $\dot{\psi}_{OS}$. β_{ST} reduces to 552 and 545 ms, respectively for RAC and RWS, compared to the 565 ms of the passive vehicle. Interestingly, $\dot{\psi}_{ST}$ for RAC increases to a value of 464 ms w.r.t. 451 ms

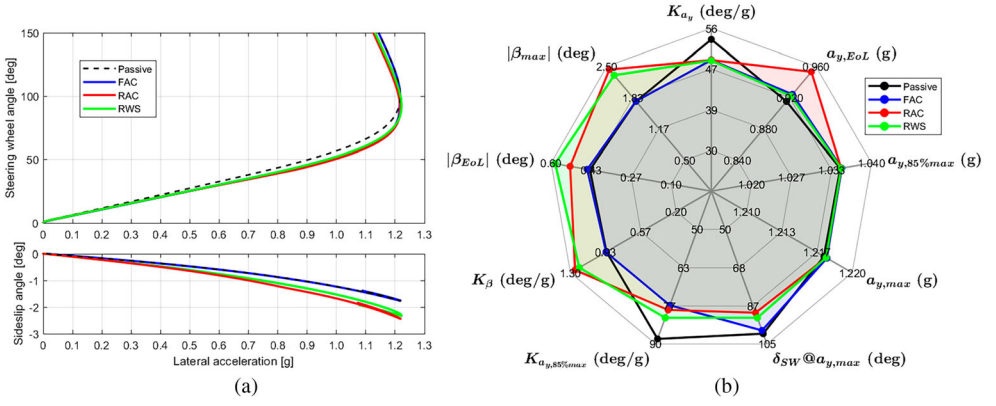

Figure 9. SPCS test results plots for the controlled vehicle with active systems: (a) understeer and sideslip curves and (b) corresponding KPIs in a spider chart.

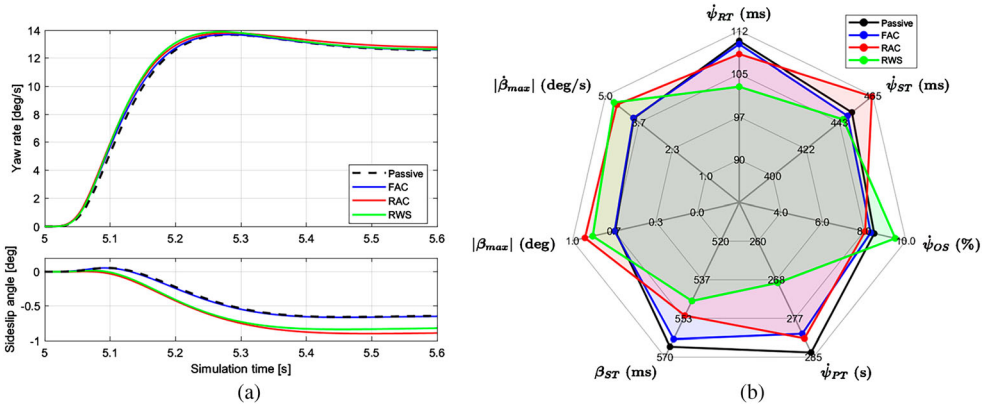

Figure 10. SI test results plots for the controlled vehicle with active systems: (a) yaw rate and sideslip angle time profiles and (b) corresponding KPIs in a spider chart.

for the passive case, which is caused by the variation of the lateral force characteristic of the rear axle.

The SSI tests in Figure 11 are performed by targeting the same maximum lateral acceleration of 0.4 g. All curves start from the same static value $G_{\dot{\psi}0}$, which is higher than the one of the passive vehicle, consistently with the understeer characteristics. RWS and RAC have a greater influence on the dynamic response. Significant differences are noticeable in the reaction times, see the values of $\Delta t_{0.5\dot{\psi}}$ and $\Delta t_{1\dot{\psi}}$, i.e. 53.7 and 60 ms for RAC, 55 and 61 ms for RWS, and 60 and 67 ms for the passive case. On the contrary, no substantial differences are observed for FAC compared to the passive vehicle. A transient performance deterioration in terms of lateral acceleration occurs with RWS and RAC, as the simplified controller leads to an increase in $\Delta t_{0.5a_y}$ and Δt_{1a_y}. The only system that manages to improve, albeit slightly, these two KPIs is FAC, with a reduction in the response time of $\sim$2 ms both at 0.5 and 1 Hz, thus meeting all the initial requirements. Once the most suitable actuation system is identified, it is possible to refine the analysis by developing a more complex control strategy, e.g. by introducing feedback control, and, above all, a more complex model of the vehicle and its actuation system.

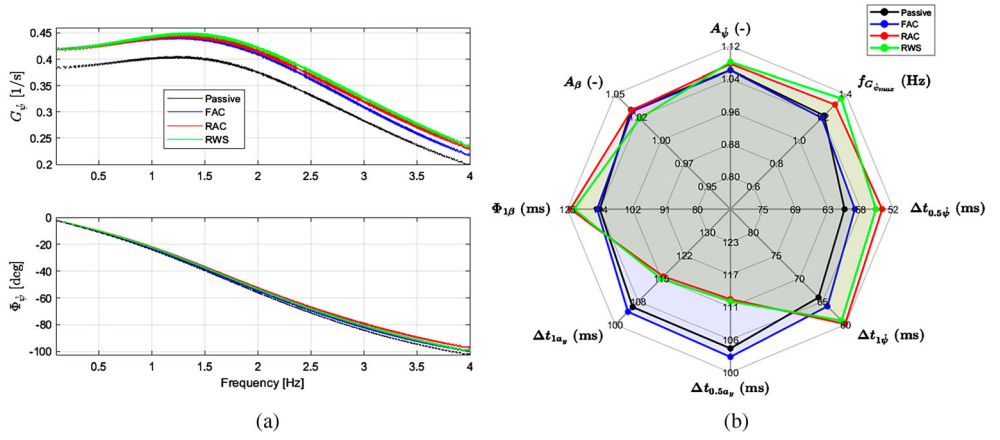

Figure 11. SSI test results plots for the controlled vehicle with active systems: (a) yaw rate frequency response characteristics and (b) corresponding KPIs in a spider chart.

6. Conclusions

The development of high-performance vehicle control strategies involves analysing the capabilities and limits of the available actuators. The assessment of the resulting feasibility region in terms of vehicle response is essential for selecting the most suitable actuator suite. The very few feasibility region studies from the literature use high-fidelity simulation tools. However, to accelerate the target setting procedure and the analysis of the pure lateral dynamics during the proof-of-concept phase, in which limited vehicle parameters are available, it would be useful to employ a simple and reliable model.

Firstly, an analysis has been conducted to determine how much simplified models with increasing levels of complexity in terms of degrees of freedom and physical accuracy deviate from a high-fidelity vehicle model in VI-CarRealTime. Standard open-loop tests, both in quasi-steady-state and transient conditions, were simulated for this purpose. The results, expressed in terms of KPIs, were compared for various simplified models, namely single-track models with linearised and nonlinear tyre behaviour, a 2-DoF two-track model, and the NLTTEK model, i.e. an augmented 3-DoF model including the yaw, sideslip, and body roll dynamics, as well as simplified suspension elasto-kinematics. NLTTEK achieves results that are very close to those of the reference high-fidelity model, and thus can support an effective feasibility region study.

Secondly, NLTTEK was used to analyse the feasibility regions of four chassis actuation systems, namely FAC, RAC, RWS, and RMD, which can modify the lateral and vertical tyre forces. The feasibility regions were found by imposing constant control actions corresponding to the respective actuation limits. The output is the locus of the achievable understeer characteristics. Different actuators have different impacts on the linear and nonlinear cornering response regions. For example, all systems, with the exception of RMD, can modify the linear response by varying the understeer gradient. RWS, FAC and RAC enable significant variations of the understeer characteristic, except for the maximum lateral acceleration, a parameter closely related to the front axle saturation, which

is not influenced by these systems. FAC and RMD maximise the lateral acceleration performance without drastically altering the sideslip angle profiles, primarily linked with the rear axle behaviour.

In conclusion, the proposed methodology allows for swift and effective decision-making during the vehicle target-setting phase, with regards to which active system/s can facilitate the achievement of specified vehicle response requirements, while considering the respective actuation constraints.

Disclosure statement

No potential conflict of interest was reported by the author(s).

References

[1] Mazzilli V, de Pinto S, Pascali L, et al. Integrated chassis control: classification, analysis and future trends. Ann Rev Control. 2021;51:172–205. doi:10.1016/j.arcontrol.2021.01.005
[2] Ataei M, Tang C, Khajepour A, et al. Active camber system for lateral stability improvement of urban vehicles. proceedings of the institution of mechanical engineers. Part D J Automobile Eng. 2019;233(14):3824–3838. doi:10.1177/0954407019832436
[3] Warth G, Frey M, Gauterin F. Usage of the cornering stiffness for an adaptive rear wheel steering feedforward control. IEEE Trans Vehicular Tec. 2018;68(1):264–275. doi:10.1109/TVT.2018.2883809
[4] Vignati M, Sabbioni E. A cooperative control strategy for yaw rate and sideslip angle control combining torque vectoring with rear wheel steering. Vehicle Syst Dyn. 2022;60(5):1668–1701. doi:10.1080/00423114.2020.1869273
[5] De Novellis L, Sorniotti A, Gruber P. Wheel torque distribution criteria for electric vehicles with torque-vectoring differentials IEEE trans. Vehicular Tec. 2013;63(4):1593–1602. doi:10.1109/TVT.2013.2289371
[6] Chatzikomis C, Sorniotti A, Gruber P, et al. Torque-vectoring control for an autonomous and driverless electric racing vehicle with multiple motors. SAE Int J Vehicle Dyn Stability NVH. 2017;1(2017-01-1597):338–351. doi:10.4271/2017-01-1597
[7] Park G, Han K, Nam K, et al. Torque vectoring algorithm of electronic-four-wheel drive vehicles for enhancement of cornering performance. IEEE Trans Vehicular Tec. 2020;69(4):3668–3679. doi:10.1109/TVT.2020.2978099
[8] Ricco M, Zanchetta M, Cardolini Rizzo G, et al. On the design of yaw rate control via variable front-to-total anti-roll moment distribution. IEEE Trans Vehicular Tec. 2019;69(2):1388–1403. doi:10.1109/TVT.2019.2955902
[9] Ruiz IR. High performance electromechanical actuator for active rear axle kinematics of a sports car. SAE Int J Passenger Car Electron Electric Syst. 2012;5(2012-01-0974):528–540. doi:10.4271/2012-01-0974
[10] Ruiz IR. Active kinematics suspension for a high performance sports car. 2013. SAE Technical Paper. (No. 2013-01-0684). doi:10.4271/2013-01-0684
[11] Marotta R, Strano S, Terzo M, et al. Active control of camber and toe angles to improve vehicle ride comfort. (SAE Technical Paper. 2022-01-0920). doi:10.4271/2022-01-0920
[12] Warth G, Frey M, Gauterin F. Design of a central feedforward control of torque vectoring and rear-wheel steering to beneficially use tire information. Vehicle Syst Dyn. 2020;58(12):1789–1822. doi:10.1080/00423114.2019.1647345
[13] Peters Y, Stadelmayer M. Control allocation for all wheel drive sports cars with rear wheel steering. Autom Eng Tech. 2019;4(3):111–123. doi:10.1007/s41104-019-00047-9
[14] Chien PC, Chen CK. Integrated chassis control and control allocation for all wheel drive electric cars with rear wheel steering. Electronics (Basel). 2021;10(22):2885–2904. doi:10.3390/electronics10222885.

[15] Dalboni M, Martins G, Tavernini D, et al. On the energy efficiency potential of multi-actuated electric vehicles. 2024. IEEE transactions on vehicular technology. in press. doi:10.1109/TVT.2024.3378154
[16] Ahmadian N, Khosravi A, Sarhadi P. Managing driving disturbances in lateral vehicle dynamics via adaptive integrated chassis control. Proc Inst Mech Eng, Part K J Multibody Dyn. 2021;235(1):122–133. doi:10.1177/1464419320977374
[17] Hu Z, Liao Y, Liu J, et al. Investigation of vehicle stability by integration of active suspension, torque vectoring, and direct yaw control. SAE Int J Vehicle Dyn Stab NVH. 2022;6(10-06-04-0029):441–459. doi:10.4271/10-06-04-0029
[18] Ahangarnejad AH, Melzi S, Ahmadian M. Integrated vehicle dynamics system through coordinating active aerodynamics control: active rear steering, torque vectoring and hydraulically interconnected suspension. Int J Autom Techn. 2019;20:903–915. doi:10.1007/s12239-019-0084-x
[19] Henning KU, Speidel S, Gottmann F, et al. Integrated lateral dynamics control concept for over-actuated vehicles with state and parameter estimation and experimental validation. Control Eng Pract. 2021;107:104704–104715. doi:10.1016/j.conengprac.2020.104704.
[20] Georgiev P, De Filippis G, Gruber P, et al. On the benefits of active aerodynamics on energy recuperation in hybrid and fully electric vehicles. Energies. 2023;16(15):5843–5870. doi:10.3390/en16155843.
[21] Chatzikomis C, Zanchetta M, Gruber P, et al. An energy-efficient torque-vectoring algorithm for electric vehicles with multiple motors. Mech Syst Signal Proces. 2019;128:655–673. doi:10.1016/j.ymssp.2019.03.012
[22] Isermann R. Automotive control: modeling and control of vehicles. 1st ed Berlin/Heidelberg: Springer; 2021.
[23] Smith DE, Starkey JM. Effects of model complexity on the performance of automated vehicle steering controllers: model development, validation and comparison. Vehicle Syst Dyn. 1995;24(2):163–181. doi:10.1080/00423119508969086
[24] Mazzilli V, Ivone D, De Pinto S, et al. On the benefit of smart tyre technology on vehicle state estimation. Vehicle Syst Dyn. 2022;60(11):3694–3719. doi:10.1080/00423114.2021.1976414
[25] Pacejka H. Tire and vehicle dynamics. 2nd ed. Oxford: Elsevier; 2005.
[26] Lenzo B, Bucchi F, Sorniotti A, et al. On the handling performance of a vehicle with different front-to-rear wheel torque distributions. Vehicle Syst Dyn. 2019;57(11):1685–1704. doi:10.1080/00423114.2018.1546013
[27] Bucchi F, Frendo F. A new formulation of the understeer coefficient to relate yaw torque and-vehicle handling. Vehicle Syst Dyn. 2016;54(6):831–847. doi:10.1080/00423114.2016.1167225
[28] Barbieri G. Automotive suspension. setting and fine-tuning of elastokinematics to improve vehicle dynamics. 1st ed Italy: Le Penseur; 2023.
[29] Henning KU, Sawodny O. Vehicle dynamics modelling and validation for online applications and controller synthesis. Mechatronics (Oxf). 2016;39:113–126. doi:10.1016/j.mechatronics.2016.08.010
[30] ISO 4138: Passenger cars – Steady-state circular driving behaviour – Open-loop test methods. International Organization for Standardization. 2012.
[31] ISO 7401: Road vehicles – Lateral transient response test methods – Open loop test methods. International Organization for Standardization. 2011.
[32] ISO 8855: Road vehicles – Vehicle dynamics and road-holding ability – Vocabulary. International Organization for Standardization. 2011.
[33] Sivaramakrishnan S, Taheri S. Using objective vehicle-handling metrics for tire performance evaluation and selection. SAE Int J Passeng Car Mech Syst. 2013;6(2013-01-0743):732–740. doi:10.4271/2013-01-0743
[34] Newland DE. An introduction to random vibrations: spectral & wavelet analysis. 3rd ed New York: Courier Corporation; 2012.